The Astrophysical Journal, 992:194 (9pp), 2025 October 20 https://doi.org/10.3847/1538-4357/ae0458

Does DESI DR2 Challenge ΛCDM Paradigm?

Himanshu Chaudhary[1], Salvatore Capozziello[2,3,4,8], Vipin Kumar Sharma[5,6], and Ghulam Mustafa[7,8]
[1] Department of Physics, Babeş-Bolyai University, Kogălniceanu Street, Cluj-Napoca, 400084, Romania; himanshu.chaudhary@ubbcluj.ro, himanshuch1729@gmail.com
[2] Dipartimento di Fisica "E. Pancini," Università di Napoli "Federico II", Complesso Universitario di Monte Sant' Angelo, Edificio G, Via Cinthia, I-80126, Napoli, Italy; capozziello@na.infn.it
[3] Istituto Nazionale di Fisica Nucleare (INFN), sez. di Napoli, Via Cinthia 9, I-80126, Napoli, Italy
[4] Scuola Superiore Meridionale, Largo S. Marcellino, I-80138, Napoli, Italy
[5] Indian Institute of Astrophysics, Koramangala II Block, Bangalore 560034, India; vipinkumar.sharma@iiap.res.in
[6] Department of Physics, Lovely Professional University, Phagwara, Punjab, 144411, India
[7] Department of Physics, Zhejiang Normal University, Jinhua 321004, People's Republic of China; gmustafa3828@gmail.com
Received 2025 July 31; revised 2025 August 28; accepted 2025 August 28; published 2025 October 15

Abstract

Although the debate about the systematic errors of DESI DR1 is still open, recent DESI DR2 is consistent with DESI DR1 and further strengthens the results of DESI DR1. In our analysis, both the LRG1 point at $z_{\rm eff} = 0.510$ and the LRG3+ELG1 point at $z_{\rm eff} = 0.934$ are in tension with the ΛCDM-anchored value of Ω_m inferred from Planck and the Type Ia supernovae compilations Pantheon$^+$, Union3, and DES-SN5YR. For luminous red galaxy 1 (LRG1) the tensions are 2.42σ, 1.91σ, 2.19σ, and 2.99σ, respectively; for LRG3+emission line galaxy 1 (ELG1) they are 2.60σ, 2.24σ, 2.51σ, and 2.96σ, respectively. From low to high redshift bins, DESI DR2 shows improved consistency relative to DESI DR1: the Ω_m tension decreases from 2.20σ to 1.84σ. However, DESI DR2 alone does not provide decisive evidence against the ΛCDM model, and the apparent signal is largely driven by specific tracers, LRG1 and LRG2. In the $\omega_0\omega_a$CDM analysis, including all tracers yields a posterior mean with $\omega_0 > -1$, which aligns with scenarios of dynamical dark energy as a potential explanation and suggests that the DESI DR2 challenges the ΛCDM paradigm. While removing LRG1 and/or LRG2 fully restores ΛCDM concordance (i.e., $\omega_0 \to -1$), we also find $\omega_0^{(\rm LRG1)} > \omega_0^{(\rm LRG2)}$, indicating LRG1 drives the apparent dynamical dark energy trend more strongly. Model selection using the natural log Bayes factor $\ln {\rm BF} \equiv \ln(\mathcal{Z}_{\Lambda\rm CDM}/\mathcal{Z}_{\omega_0\omega_a\rm CDM})$ shows weak evidence for ΛCDM when LRG1, LRG2, or both are removed, and it is inconclusive for the full sample; thus, the data do not require the extra ω_a freedom, and the apparent $\omega_0 > -1$ preference should be interpreted cautiously as a manifestation of the ω_0–ω_a degeneracy under limited per tracer information.

Unified Astronomy Thesaurus concepts: Cosmological evolution (336); Cosmology (343)

1 Introduction

Many different observational probes and experiments have been conducted over the years in order to interpret the dark energy (DE) fluid (A. G. Riess et al. 1998; S. Perlmutter et al. 1999; K. Bamba et al. 2012). A comprehensive analysis of cosmological data sets at different redshifts is paramount to understanding its properties, with a rule of thumb of testing as many ranges as possible. Whenever both baryon acoustic oscillations (BAO) and supernovae (SNe) deviate significantly from ΛCDM predictions at the same redshift range, this provides strong phenomenological evidence that DE is dynamic rather than a cosmological constant (A. Notari et al. 2025; V. K. Sharma et al. 2025; A. Sousa-Neto et al. 2025).

The ΛCDM model is widely regarded as the best model for explaining most cosmological observations despite its degeneracies at the theoretical level (Y. B. Zel'dovich 1968; S. Weinberg 1989). However, using their first year data, the DESI collaboration (R. Calderon et al. 2024; A. G. Adame et al. 2025; M. A. Karim et al. 2025; K. Lodha et al. 2025) has found that DE is evolving at a $\geqslant 3\sigma$ significance level. This result will inevitably bring the shifts of the best-fit values of relevant ΛCDM cosmological parameters. Therefore, modeling the DE through parameterization is one of the most direct ways to understand its dynamical behavior in a model-independent approach (M. Chevallier & D. Polarski 2001; E. V. Linder 2003; V. Sahni & A. Starobinsky 2006; C.-G. Park et al. 2024; W. J. Wolf et al. 2025a, 2025b). This makes model-independent techniques an attractive route to discover DE properties at a deeper level (S. Vilardi et al. 2025). In this paper, we want to perform our analysis for different redshift ranges and compare the DESI DR1 and DR2 predictions for the ΛCDM model and $\omega_0\omega_a$CDM model.

Our paper is organized as follows. In Section 2, we introduce the cosmological background equations and models. Section 3 details the core of this work with data sets and methodology using Markov Chain Monte Carlo (MCMC) sampling against the publicly available DESI DR2 data, while Section 4 is dedicated to the discussion of results. We discuss the implications of our results and conclusions in Section 5.

2 Cosmological Background and Models

Considering the spatially flat Friedmann–Lemaître–Robertson–Walker (FLRW) universe at relatively late times, that is $z << 10^2$, where the density of radiation can be safely ignored; the first Friedmann equation reads

$$H^2 = \frac{8\pi G}{3}(\rho_{\rm m,0}a^{-3} + \rho_{\rm de}). \quad (1)$$

[8] Corresponding author.

The continuity equation in FLRW is

$$\dot{\rho}_{\rm x} + 3H(1 + w_{\rm x})\rho_{\rm x} = 0, \tag{2}$$

where $\rho_{\rm x}$ represents the energy density of each component with x$\in$ (de, m), over (.) represents the cosmic time derivative, and $w_{\rm x}$ represents the equation of state (EoS) parameter. Here, "de" and "m" are the DE and the matter components, respectively.

Suppose that we parameterize $w(a)$, so that the evolution of DE ($\rho_{\rm de}$) within Equation (1) is the following solution of Equation (2):

$$\rho_{\rm de} = \frac{\rho_{\rm de,0}}{a^3}\exp\left(-3\int_1^a \frac{w_{\rm de}(a')}{a'}\,da'\right), \tag{3}$$

where $\rho_{\rm de,0}$ is the present value of the DE density. With a particular form choice $w_{\rm de}(a)$ (Equation (1)), it can be used to determine the cosmological evolution.

In principle, there is no dictum that specifies the best parameterizations. Nevertheless, by using observational data, it is possible to find parameterizations that are cosmologically viable. Let us now outline the ΛCDM model and its straightforward dynamic improvement represented by the $\omega_0\omega_a$CDM model.

2.1 ΛCDM Model

This is the standard concordance cosmological model characterized by constant EoS, $w_{\rm de} = -1$. Equation (3) gives $\rho_{\rm de} = \rho_{\rm de,0}$. The dimensionless Hubble function for flat FLRW universe reads

$$E(z)^2\left(\equiv\frac{H(z)}{H_0}\right)^2 = \Omega_m(1 + z)^3 + (1 - \Omega_m). \tag{4}$$

2.2. $\omega_0\omega_{\rm a}$CDM Model

It is possible to approximate the behavior of several DE models by using the function $w_{\rm de}$ in a model-independent way, but with time-dependent parameterizations.

Specifically, we consider the two-parameter model ($\omega_0\omega_a$CDM) with the following free parameters: ω_0, which represents the current value of $\omega_{\rm de}(a)$, and $w_a = -\frac{dw_{\rm de}(a)}{da}\,|_{a=a_0}$, which quantifies dynamical characteristics of $\omega_{\rm de}(a)$. The standard ΛCDM model can be recovered for the choices $\omega_0 = -1$ and $\omega_a = 0$. In this aspect, model-independent techniques applied to observational data provide an interesting approach to understanding DE properties in more detail. To this category belong the popular Chevallier–Polarski–Linder (CPL) ansatz (M. Chevallier & D. Polarski 2001; E. V. Linder 2003; A. Chudaykin et al. 2021; C.-G. Park et al. 2024) for the DE EoS, defined as

$$\omega(z) = \omega_0 + \frac{z}{1 + z}\omega_a = \omega_0 + \omega_a(1 - a). \tag{5}$$

Equation (3) gives

$$\rho_{\rm de} = \rho_{\rm de,0}(1 + z)^{3(1+w_0+w_a)}\exp\left(-\frac{3w_a z}{1 + z}\right). \tag{6}$$

The corresponding Hubble function is given by C. Escamilla-Rivera & S. Capozziello (2019):

$$E(z)^2 = \Omega_m(1 + z)^3 + \Omega_x(1 + z)^{3(1+\omega_0+\omega_a)}e^{-\frac{3\omega_a z}{1+z}}. \tag{7}$$

The $\omega_0\omega_a$CDM model is widely used because of its flexibility and robust behavior in describing the evolution of DE.

The next section scrutinizes both models based on the DESI DR2 data sets.

3 Data Set and Methodology

Let us consider now the recent measurements of BAO from more than 14 million galaxies and quasars taken from DESI DR2[9] (M. A. Karim et al. 2025). These data have been extracted from various tracers, including bright galaxy sample (BGS), luminous red galaxies (LRG1–3), emission line galaxies (ELG1 and ELG2), quasi-stellar objects (QSOs), and Lyα forests.

To analyze these data, we employ the nested sampling algorithm, a Bayesian inference technique well-suited for navigating complex, high-dimensional parameter spaces. Nested sampling transforms the challenging multidimensional integration of the Bayesian evidence into a more manageable one-dimensional integral over the prior volume. This method not only enables efficient parameter estimation but also facilitates the computation of Bayesian evidence, $\mathcal{Z} = p(D|M)$, which is crucial for model comparison.

For the nested sampling implementation, we use the PyPolyChord library[10] (W. Handley et al. 2015a, 2015b), which is optimized for high-dimensional spaces and can handle multimodal posterior distributions through clustering techniques. In our analysis, we apply uniform priors to the model parameters, which are implemented via PyPolyChord's `UniformPrior` class. We consider two cosmological models: the standard ΛCDM model and the $\omega_0\omega_a$CDM model. For both models, we specify appropriate priors on their parameters. In the case of the ΛCDM model, we use uniform priors on the following parameters: $H_0 \in [50, 100]\,{\rm km\,s^{-1}\,Mpc^{-1}}$, $\Omega_{m0} \in [0, 1]$, and $r_d \in [100, 200]$ Mpc. For the $\omega_0\omega_a$CDM model, we use the following uniform priors $\omega_0 \in [-3, 1]$ and $\omega_a \in [-3, 2]$, with the additional condition that $\omega_0 + \omega_a < 0$.

To efficiently explore the parameter space and detect multiple posterior modes, we configure PyPolyChord to use 300 live points with clustering enabled. For analyzing and visualizing the results, we utilize the `getdist` package[11] (A. Lewis 2025), which generates detailed marginalized posterior distributions and parameter correlation plots. To analyze the BAO data set, we need to compute two important distance measures: the Hubble distance

$$D_H(z) = \frac{c}{H(z)}, \tag{8}$$

and the comoving angular diameter distance

$$D_M(z) = \frac{c}{H_0}\int_0^z \frac{dz'}{H(z')}, \tag{9}$$

[9] https://github.com/CobayaSampler/bao_data
[10] https://github.com/PolyChord/PolyChordLite
[11] https://github.com/cmbant/getdist

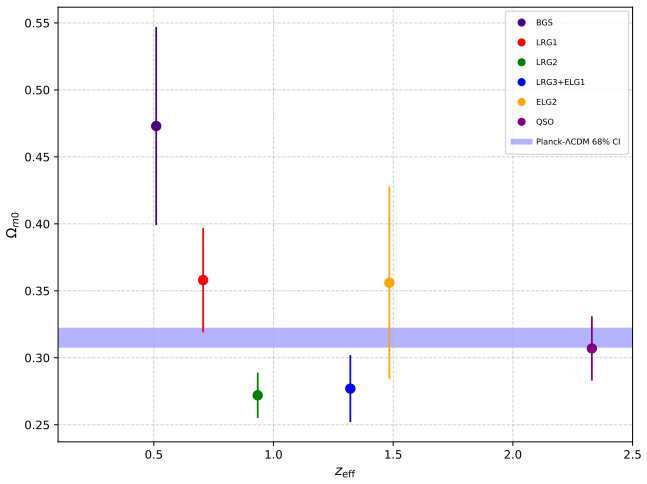

Figure 1. The figure shows the values of Ω_m at 68% confidence intervals for different $z_{\rm eff}$ values. The blue band represents the Planck ΛCDM prediction for Ω_m.

and the volume-averaged distance

$$D_V(z) = [zD_M^2(z)D_H(z)]^{1/3}. \quad (10)$$

These distances are then used to calculate the ratios $D_H(z)/r_d$, $D_M(z)/r_d$, and $D_V(z)/r_d$ which we compare directly with observational data. These calculated values are then compared with the predictions made by the observations.

Furthermore, we also calculate the following ratio:

$$\frac{D_M/r_d}{D_H/r_d} = \int_0^z \frac{1}{E(z')}\, dz'. \quad (11)$$

This approach is independent of the sound horizon r_d. The ratio $\frac{D_M\,/\,r_d}{D_H\,/\,r_d}$ involves the angular diameter distance D_M and the Hubble distance D_H, both normalized by r_d. This ratio depends on the function $E(z)$. The data set for $\frac{D_M}{D_H}$ can be found in Table 4, column (6) of M. A. Karim et al. (2025), corresponding to each tracer. For each tracer, one can compute the model value $\frac{D_M}{D_H}_{\rm Model}$ and compare it with the observational data set using the standard likelihood function. The likelihood function to compare the model prediction $\frac{D_M}{D_H}_{\rm Model}$ with the observational data $\frac{D_M}{D_H}_{\rm Obs}$ is given by

$$\mathcal{L}(\theta) = \prod_i \exp\left[-\frac{1}{2}\left(\frac{\frac{D_M}{D_H}_{{\rm Obs},i} - \frac{D_M}{D_H}_{{\rm Model},i}(\theta)}{\sigma_i}\right)^2\right], \quad (12)$$

where $\frac{D_M}{D_H}_{{\rm Obs},i}$ is the observed ratio for the ith tracer, $\left(\frac{D_M}{D_H}\right)_{{\rm Model},i}(\boldsymbol{\theta})$ is the predicted ratio for the ith tracer based on the cosmological model with parameter set $\boldsymbol{\theta} = \{\Omega_m, H_0, \omega_0, \omega_a, r_d, \ldots\}$, and σ_i is the uncertainty associated with the ith observed data point. It is important to note that, in our analysis, r_d is treated as a free parameter (L. Pogosian et al. 2020, 2024; K. Jedamzik et al. 2021; W. Lin et al. 2021; S. Vagnozzi 2023). We then construct the derived quantity $h\,r_d$ (with $h \equiv H_0/100$) and obtain its posterior by propagating the MCMC samples of h and r_d sample by sample.

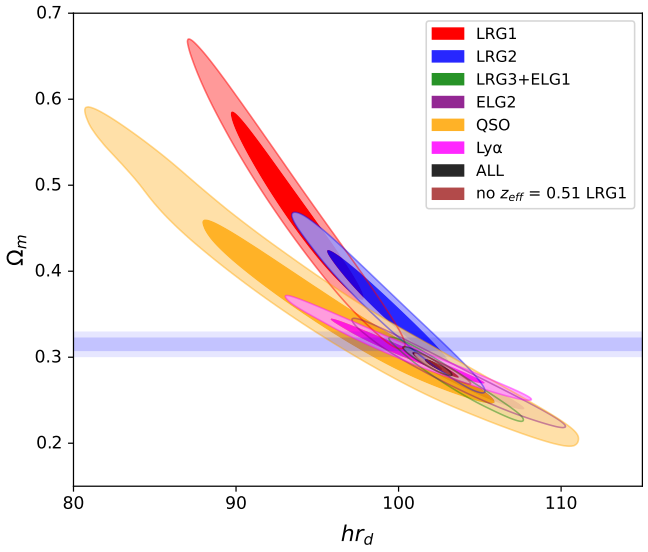

Figure 2. The figure shows the posterior distributions of different tracers corresponding to different $z_{\rm eff}$ from the DESI DR2 data set within the ΛCDM model. These are presented at 68% (1σ) and 95% (2σ) confidence levels in the Ω_m–hr_d contour plane. The blue band represents the Planck ΛCDM prediction for Ω_m.

Table 1
The Table Shows the Values of Ω_m and hr_d at 68% (1σ) and 95% (2σ) Confidence Intervals, Obtained from Different Tracers Using DESI DR2 Measurements

Tracer	$z_{\rm eff}$	hr_d	Ω_m
LRG1	0.510	$93.64^{\pm5.502}_{\pm2.703}$	$0.473^{\pm0.132}_{\pm0.065}$
LRG2	0.706	$99.24^{\pm4.420}_{\pm2.207}$	$0.358^{\pm0.075}_{\pm0.032}$
LRG3+ELG1	0.934	$103.50^{\pm3.162}_{\pm1.558}$	$0.272^{\pm0.036}_{\pm0.015}$
ELG2	1.321	$103.56^{\pm5.262}_{\pm2.637}$	$0.277^{\pm0.047}_{\pm0.021}$
QSO	1.484	$96.04^{\pm12.206}_{\pm6.197}$	$0.356^{\pm0.130}_{\pm0.061}$
Lyα	2.330	$100.29^{\pm5.871}_{\pm3.201}$	$0.307^{\pm0.046}_{\pm0.021}$
All	⋯	$101.79^{\pm1.172}_{\pm0.611}$	$0.297^{\pm0.013}_{\pm0.007}$
No $z_{\rm eff} = 0.510$ LRG1	⋯	$102.59^{\pm1.449}_{\pm0.700}$	$0.287^{\pm0.013}_{\pm0.007}$

Note. In this table, we do not consider the BGS data point.

4 Results

Figure 1 shows the values of Ω_m at different $z_{\rm eff}$ values. We observe that the predicted value of Ω_m using the LRG1 data set, corresponding to $z_{\rm eff} = 0.51$, deviates from the Planck-ΛCDM confidence interval represented by the blue band. Figure 2 shows the posterior distributions of different tracers at 1σ and 2σ confidence intervals, obtained from various $z_{\rm eff}$ measurements using DESI DR2 data sets. Notably, one can observe that the contours for the LRG1 data set do not lie within the blue band, which represents the Planck ΛCDM prediction for Ω_m.

Table 1 highlights two main points. First, the LRG1 data at $z_{\rm eff} = 0.510$ yield an unexpectedly high value of Ω_m compared to the Planck prediction, $\Omega_m = 0.315 \pm 0.007$N. (Aghanim et al. 2020). In DESI DR2, LRG1 predicts $\Omega_m = 0.473 \pm 0.065$, corresponding to a $\sim 2.42\sigma$ discrepancy with the Planck prediction. Other redshift bins also show tensions with the Planck prediction: LRG2 ($z_{\rm eff} = 0.760$) predicts $\Omega_m = 0.358 \pm 0.032$ (1.31σ); LRG3+ELG1 ($z_{\rm eff} = 0.934$) gives $\Omega_m = 0.272 \pm 0.015$ (2.60σ); ELG2 ($z_{\rm eff} = 1.321$) yields

$\Omega_m = 0.277 \pm 0.021$ (1.72σ); QSO ($z_{\rm eff} = 1.484$) gives $\Omega_m = 0.356 \pm 0.061$ (0.67σ); and Lyα ($z_{\rm eff} = 2.330$) shows only a 0.36σ tension. These findings indicate that the LRG1 discrepancy at $z_{\rm eff} = 0.510$ is not unique, as other tracers, most notably LRG3+ELG1 at $z_{\rm eff} = 0.934$, show even stronger deviations from the Planck prediction. More broadly, all tracers except Lyα exhibit some level of tension, with a pattern that is complex and not monotonic in redshift. A similar trend is observed in Table 1 of E. Ó Colgáin et al. (2026), where the predicted values of Ω_m in different redshift bins also exhibit discrepancies with the Planck prediction.

Consequently, these values also show discrepancies with various Type Ia supernovae (SNe Ia) measurements: Pantheon$^+$ ($\Omega_m = 0.334 \pm 0.018$; D. Brout et al. 2022), Union3 ($\Omega_m = 0.356^{+0.028}_{-0.026}$; D. Rubin et al. 2025), and DES-SN5YR ($\Omega_m = 0.352 \pm 0.017$; T. Abbott et al. 2024). For DESI DR2, the LRG1 sample exhibits tensions of approximately 2.06σ, 1.67σ, and 1.80σ with these three data sets, respectively. In comparison, the LRG3+ELG1 sample shows even larger tensions of about 2.24σ, 2.51σ, and 2.96σ. Note that these SNe Ia samples typically have low effective redshifts around $z_{\rm eff} \sim 0.3$.

This trend extends beyond the Planck and SNe Ia calibrations. At $z_{\rm eff} = 0.510$, Sloan Digital Sky Survey (SDSS)-IV data predict $\Omega_m \sim 0.340 \pm 0.09$ (E. Ó Colgáin et al. 2022), while DESI DR1 predicts $\Omega_m \sim 0.67^{+0.18}_{-0.17}$ (E. Ó Colgáin et al. 2026). In comparison, the DESI DR2 measurement at the same redshift shows a tension of approximately 1.20σ with SDSS-IV and 1.08σ with DESI DR1, indicating a deviation across different surveys. A similar discrepancy is observed within the DESI DR1 and DESI DR2 measurements at $z_{\rm eff} = 0.706$. Using DESI DR1 data, (E. Ó Colgáin et al. 2022) predicted $\Omega_m = 0.219^{+0.087}_{-0.069}$ (see Table 1). However, DESI DR2 measurements at the same redshift give $\Omega_m \sim 0.358 \pm 0.032$, showing an increase of approximately 1.83σ. These predictions also show a similar discrepancy when compared to the value $\Omega_m = 0.49 \pm 0.11$ predicted by E. Ó Colgáin et al. (2026) at $z_{\rm eff} = 0.706$ using SDSS-IV. The comparison between DESI DR1 and this value shows a discrepancy of 2.09σ, while the comparison between DESI DR2 and E. Ó Colgáin et al. (2026) shows a discrepancy of 1.14σ. It is worth noting that DESI DR1 and DESI DR2 agree with the predicted value of Ω_m at $z_{\rm eff} = 0.934$ and only show a tension of about 0.10σ.

The second notable feature is the negative correlation between Ω_m and hr_d, as shown in Figure 2, which shows the Ω_m–hr_d contour planes for the various DESI DR2 tracers. This negative correlation has already been well observed in different BAO analyses (D. J. Eisenstein et al. 2005; W. J. Percival et al. 2010; É. Aubourg et al. 2015; S. Alam et al. 2017, 2021), observational Hubble data (OHD; M. G. Dainotti et al. 2022b; E. Ó Colgáin et al. 2024), SNe Ia (M. G. Dainotti et al. 2021; E. Ó Colgáin et al. 2022, 2024; J.-P. Hu & F.-Y. Wang 2022; J. Wagner 2022; X. Jia et al. 2023; E. Pastén & V. H. Cárdenas 2023; M. Dainotti et al. 2023a; M. Malekjani et al. 2024), combinations of OHD and SNe Ia (C. Krishnan et al. 2020; E. Ó Colgáin et al. 2024), gamma-ray bursts (GRBs; M. G. Dainotti et al. 2022c; G. Bargiacchi et al. 2025), standardizable QSOs (G. Risaliti & E. Lusso 2019; E. Lusso et al. 2020; E. Ó Colgáin et al. 2022, 2024; S. Pourojaghi et al. 2022; M. G. Dainotti et al. 2022a, 2023c; G. Bargiacchi et al. 2023), and discussions on strong lensing time delays in lensed QSOs (M. Millon et al. 2020; A. J. Shajib et al. 2020; K. C. Wong et al. 2020) and SNe Ia (P. L. Kelly et al. 2023; M. Pascale et al. 2025). This is clearly shown in Figure 5 of M. Millon et al. (2020) (see also X. Li & K. Liao 2024), where the error bars for H_0 from SN Refsdal and SN H0pe do not overlap, indicating a disagreement of about 1.5σ. It is important to note that SN H0pe has a lens redshift of $z = 0.35$, while SN Refsdal has a lens redshift of $z = 0.54$. This makes the trend observed in Figure 5 of M. Millon et al. (2020) consistent with the decreasing trend of H_0 with lens redshift, as originally reported the appendix of an article by K. C. Wong et al. (2020).

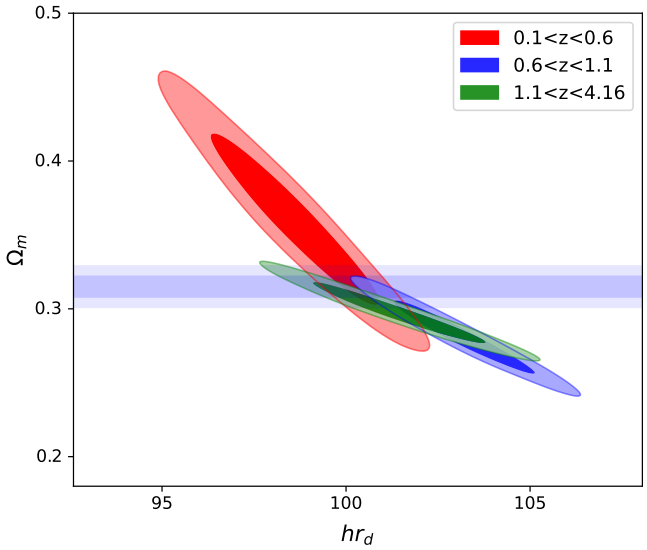

Figure 3. The figure shows the posterior distributions at 68% (1σ) and 95% (2σ) in the Ω_m–hr_d plane using different redshift bins from the DESI DR2 compilation. The blue band represents the Planck ΛCDM prediction for Ω_m.

A growing body of work is either questioning (N. Khadka & B. Ratra 2020, 2021; V. Petrosian et al. 2022; J. Singal et al. 2022; M. Zajaček et al. 2024) or improving the Risaliti Lusso standardizable QSO prescription (G. Bargiacchi et al. 2022; M. G. Dainotti et al. 2022a, 2024a, 2024b; M. Benetti et al. 2025). Despite these corrections, residual evolution in the Ω_m parameter is still reported (A. Ł. Lenart et al. 2023; M. G. Dainotti et al. 2024a, 2024b; D. Camarena et al. 2025). Additionally, dark energy survey (DES) SNe, which have a higher effective redshift (T. Abbott et al. 2024), show a larger Ω_m, consistent with these observations. Moving beyond traditional probes, like SNe, QSOs (G. Risaliti & E. Lusso 2019; E. Lusso et al. 2020), and GRBs (M. G. Dainotti et al. 2008; M. Demianski et al. 2017; G. P. Srinivasaragavan et al. 2020; N. Khadka et al. 2021; M. Dainotti et al. 2023b; A. C. Alfano et al. 2024) calibrated by SNe, may also yield higher Ω_m values at higher redshifts. This could be due to large data scatter rather than any variation in ΛCDM parameters. Comparing SNe in overlapping redshift ranges can help distinguish between these possibilities (E. Ó Colgáin et al. 2022). Returning to the main point, each $z_{\rm eff}$ from DESI DR2 further supports the negative correlation between Ω_m and hr_d, which is also evident in Figure 2, where the posterior distributions for each tracer are tilted from the top left to the bottom right.

In Figure 3, we show the posterior distributions of the Ω_m–hr_d plane at the 1σ and 2σ confidence levels, using different redshift bins from the DESI DR2 compilation. Table 2 shows the corresponding numerical values obtained

Table 2
This Table Shows the Values of Ω_m at 68% (1σ) and 95% (2σ) Confidence for Different Redshift Bins, Derived from DESI DR2 Measurements

Redshift Range (z)	$H_0 r_d$ (100 km s^{-1})	Ω_m
$0.1 < z < 0.6$	$93.50^{\pm 3.021}_{\pm 1.588}$	$0.362^{\pm 0.073}_{\pm 0.041}$
$0.6 < z < 1.1$	$103.16^{\pm 2.465}_{\pm 1.254}$	$0.281^{\pm 0.030}_{\pm 0.016}$
$1.1 < z < 4.16$	$101.45^{\pm 3.033}_{\pm 1.454}$	$0.297^{\pm 0.024}_{\pm 0.013}$

for Ω_m and hr_d at those redshift bins. One can observe that in the Ω_m–hr_d plane, the ΛCDM yields different preferred values of Ω_m across redshift bins, without a clear monotonic pattern. These variations are more naturally interpreted as statistical fluctuations and parameter degeneracies than as evidence for a true physical redshift evolution of Ω_m. The corresponding numerical values can be seen in the third column of Table 2. Statistically speaking, the matter density parameter Ω_m shows a discrepancy of approximately 1.84σ when moving from the low redshift bin to the higher redshift bin, and a discrepancy of 0.78σ when moving from the high redshift bin to an even higher redshift bin. On the other hand, in the same plane, the product hr_d initially predicts low values at low redshift bins, increases to intermediate values in intermediate redshift bins, and then decreases again at larger redshift bins. Indeed, Ω_m and hr_d exhibit a negative correlation.

The DESI DR2 data set shows some improvement when moving from higher to even higher redshifts, compared to the DESI DR2 predictions in E. Ó Colgáin et al. (2026) (see Table 2). The authors computed the value of Ω_m at different redshift bins and found that at low redshift, they predict $\Omega_m = 0.459 \pm 0.098$. At higher redshifts, they predict $\Omega_m = 0.231 \pm 0.033$, and at even higher redshift bins, they found $\Omega_m = 0.324 \pm 0.038$. Statistically, the matter density at low redshift shows a tension of about 2.20σ, and when moving from the high to even higher redshift bins, the tension is about 1.85σ.

Note that at around 2σ, one might consider disregarding these results. However, it is well established that the matter density in the ΛCDM Universe is approximately 30%. Based on the DESI DR2 results, there is now a region of the Universe, particularly at lower redshifts, where the matter density reaches 47.3%, compared to about 65% in light of the DESI DR1 predictions. This is strikingly inconsistent with the standard model.

In our analysis, using the full DESI DR2 compilation, we obtain $\Omega_m = 0.297 \pm 0.007$. This value is in tension with Planck, Pantheon$^+$, Union3, and DES-SN5YR at approximately 1.82σ, 1.92σ, 2.19σ, and 2.99σ, respectively. While all of these differences remain below the 3σ threshold, they are nonetheless significant and warrant further investigation. When we exclude the LRG1 tracers, we obtain a lower value of $\Omega_m = 0.289 \pm 0.007$, which increases the tensions to 2.83σ, 2.43σ, 2.56σ, and 3.54σ with Planck, Pantheon$^+$, Union3, and DES-SN5YR, respectively. These results clearly show that removing LRG1 increases the tension with Planck from 1.82σ to 2.83σ, indicating that LRG1 actually pulls the combined result closer to the Planck prediction rather than driving it away.

The assumption that Ω_m is constant in ΛCDM is challenged by mild tensions across tracers, with some approaching the 3σ level. Given the underconstrained nature of tracer-wise fits, such tensions should be interpreted with caution, as they may arise from systematic effects or model degeneracies rather than genuine deviations from ΛCDM. This issue must be understood within a broader context, alongside the existing tension in H_0, which suggests a potential problem in the background cosmology. There is also the tension in $S_8 = \sigma_8\sqrt{\Omega_m/0.3}$. While these may seem like separate issues, it is crucial to recognize that they could be interconnected, especially if discrepancies in Ω_m are confirmed (Ö. Akarsu et al. 2024). The reason is that H_0 is correlated with Ω_m at the background level in the late Universe, and S_8 is clearly dependent on Ω_m. Therefore, if Ω_m is not constant in the ΛCDM model, the tensions in H_0 and S_8 are likely symptoms of the same underlying issue.

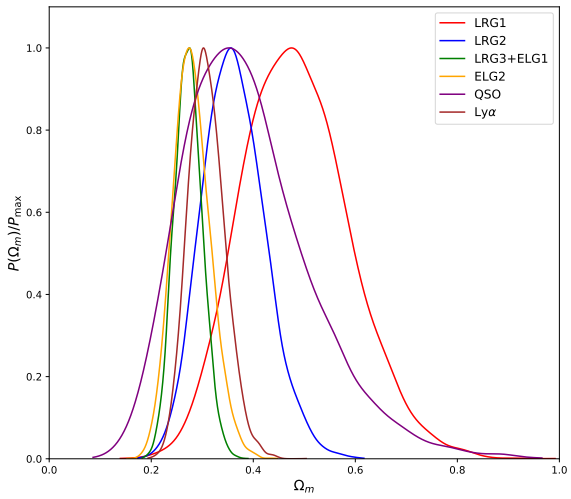

Figure 4. The figure shows the normalized probability distribution of Ω_m for different tracers at various effective redshifts $z_{\rm eff}$, independent of the hr_d dependence

Table 3
Values of Ω_m for Different Tracers at Various Effective Redshifts $z_{\rm eff}$, Independent of the hr_d Dependence

Tracer	$z_{\rm eff}$	Ω_m
LRG1	0.510	0.485 ± 0.011
LRG2	0.706	0.363 ± 0.054
LRG3+ELG1	0.934	0.273 ± 0.026
ELG2	1.321	0.280 ± 0.032
QSO	1.484	0.389 ± 0.014
Lyα	2.330	0.309 ± 0.031
All	⋯	0.299 ± 0.013
No $z_{\rm eff} = 0.51$ LRG1	⋯	0.292 ± 0.012

Table 3 shows the values of Ω_m using the D_M/D_H measurements at different BAO tracers. This approach is intended to remove the dependence on $H_0 r_d$, allowing for a more direct constraint on Ω_m. It was expected that this method would yield smaller errors; however, this was not the case. We again observe an anomaly in the DESI DR2 LRG1 data, as evident in Figure 4. Specifically, the LRG1 data at $z_{\rm eff}$ yield a higher value of Ω_m, indicating that the issue continues.

From the above discussion, it has been confirmed that the value of Ω_m at $z_{\rm eff} = 0.51$ using the LRG1 data set shows a strong disagreement with the Planck-ΛCDM model, with a discrepancy of about 2.12σ. It has also been shown that this constraint on Ω_m disagrees with the Pantheon$^+$ compilation at the 2.3σ level, despite SNe Ia being highly sensitive to similar redshift ranges. These disagreements between the DESI and

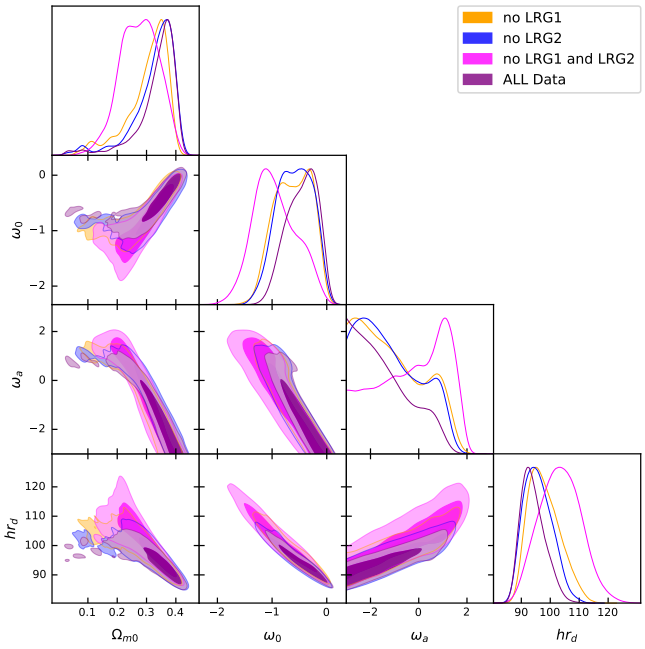

Figure 5. The figure shows the confidence contours at the 68% (1σ) and 95% (2σ) levels for the $\omega_0\omega_a$CDM model, using no LRG1, no LRG2, no LRG1 and LRG2, and the full DESI DR2 sample.

Pantheon$^+$ SNe Ia data sets, along with other SNe Ia data sets, which all generally agree on $\Omega_m \sim 0.3$ at lower redshifts, call for further investigation.

4.1 Constraints on the $\omega_0\omega_a$CDM Model

In this subsection, we constrain the parameters of the $\omega_0\omega_a$CDM model using the DESI DR2 data set alone. Figure 5 shows the constraints on the $\omega_0\omega_a$CDM model using the DESI DR2 data set, both with and without the LRG1 and LRG2 data sets, as well as excluding both simultaneously. The corresponding numerical results from the MCMC analysis are summarized in Table 4. When we exclude the LRG1 data set, the $\omega_0\omega_a$CDM model yields $\omega_0 = -0.52 \pm 0.31$. A similar trend can be observed when E. Ó Colgáin et al. (2026) consider the DESI DR1 data set. They obtain $\omega_0 = -0.560^{+0.266}_{-0.384}$ with the LRG1 data set included, and $\omega_0 = -0.984^{+0.427}_{-0.422}$ when the LRG1 sample is excluded. Removing the LRG2 data set while keeping LRG1 gives $\omega_0 = -0.46 \pm 0.29$. When both LRG1 and LRG2 are excluded, we obtain $\omega_0 = -0.99 \pm 0.37$, and for the full DESI DR2 compilation, we find $\omega_0 = -0.41 \pm 0.20$. It is important to note that whenever LRG1 and/or LRG2 are included, the inferred ω_0 deviates significantly from the ΛCDM prediction ($\omega_0 = -1$). By contrast, when both LRG1 and LRG2 are removed, the estimate shifts back toward $\omega_0 = -1$, fully restoring concordance with the ΛCDM model.

These results provide three key insights. First, DESI DR2 shows deviations from ΛCDM concordance, suggesting the possibility of evolving DE with $\omega_0 > -1$. Second, this apparent evolution is largely driven by the LRG1 and LRG2 samples. Third, what drives the evolving DE signal in DR2 is actually the combination of a high Ω_m (LRG1), a lower Ω_m (LRG2), and a higher Ω_m at higher redshift; combined, these effects produce the observed signal. E. Ó Colgáin et al. (2025) (see Figure 4) also predict similar trends: the faded blue curve corresponds to DESI DR1, while the dark blue line corresponds to DESI DR2. They further find that, in DESI DR2, the LRG2 tracer contributes more strongly than LRG1 to the dynamical DE signal. The role of LRG2 is also discussed further in the appendix of S. Goldstein et al. (2025).

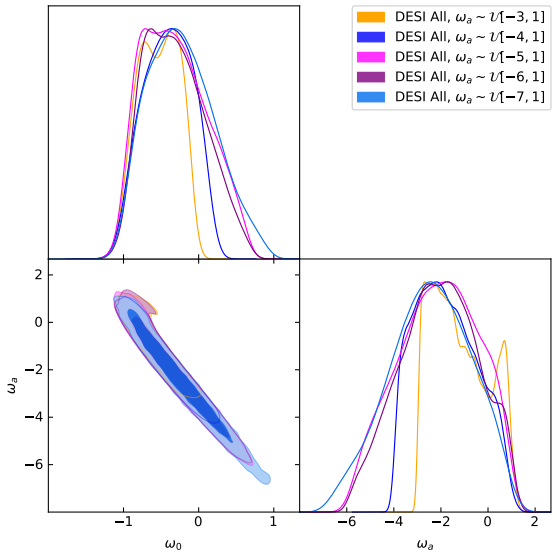

Figure 6. The figure shows the prior sensitivity of the $\omega_0\omega_a$CDM constraints from DESI DR2.

Table 4
Constraints on the Parameters of the ΛCDM and $\omega_0\omega_a$CDM Models from DESI DR2 at 68% (1σ) and 95% (2σ) Confidence Levels, Based on the Full Data Set as Well as Cases Excluding the LRG1 and/or LRG2 Redshift Data Points

Parameter	Data Set	ΛCDM	$\omega_0\omega_a$CDM
Ω_{m0}	No LRG1	$0.287^{\pm0.013}_{\pm0.007}$	$0.33^{\pm0.16}_{\pm0.02}$
	No LRG2	$0.298^{\pm0.013}_{\pm0.006}$	$0.36^{\pm0.08}_{\pm0.03}$
	No LRG1 and LRG2	$0.291^{\pm0.015}_{\pm0.008}$	$0.26^{\pm0.14}_{\pm0.06}$
	DESI DR2	$0.297^{\pm0.013}_{\pm0.007}$	$0.36^{\pm0.03}_{\pm0.02}$
ω_0	No LRG1	⋯	$-0.52^{\pm0.66}_{\pm0.31}$
	No LRG2	⋯	$-0.46^{\pm0.61}_{\pm0.29}$
	No LRG1 and LRG2	⋯	$-0.99^{\pm0.63}_{\pm0.37}$
	DESI DR2	⋯	$-0.41^{\pm0.48}_{\pm0.20}$
ωa	No LRG1	⋯	$-1.66^{\pm1.24}_{\pm0.92}$
	No LRG2	⋯	$-1.71^{\pm1.22}_{\pm0.97}$
	No LRG1 and LRG2	⋯	$-0.19^{\pm2.60}_{\pm1.69}$
	DESI DR2	⋯	$-1.99^{\pm0.93}_{\pm0.69}$
hrd	No LRG1	$102.59^{\pm1.44}_{\pm0.70}$	$96.69^{\pm6.67}_{\pm4.12}$
	No LRG2	$101.20^{\pm1.30}_{\pm0.54}$	$93.93^{+5.}_{\pm3.77}$
	No LRG1 and LRG2	$102.04^{\pm1.75}_{\pm0.83}$	$104.77^{\pm11.36}_{\pm7.29}$
	DESI DR2	$101.79^{\pm1.17}_{\pm0.61}$	$93.29^{\pm3.79}_{\pm2.42}$
lnBF	No LRG1	0	2.41
	No LRG2	0	2.06
	No LRG1 and LRG2	0	1.89
	DESI DR2	0	0.10

In Figure 6, we also show that when the full DESI DR2 data are used and the prior on ω_a is widened, in each case ω_a is pushed to large negative values exceeding the prior limits in order to accommodate $\omega_0 > -1$ (see also M. Cortês & A. R. Liddle 2024). Recent studies likewise find that relaxing the prior on ω_a can drive ω_0 to larger values, up to $\omega_0 \sim 1$

(D. Wang 2024b), which is incompatible with late-time accelerated expansion ($\omega(z) < -1/3$). This behavior indicates sensitivity to prior volume along the ω_0–ω_a degeneracy under limited per-tracer information; therefore, the apparent preference for $\omega_0 > -1$ should not be interpreted as a data-driven detection. To assess whether the extra freedom is warranted, we report the (natural) log Bayes factor, $\ln \mathrm{BF} \equiv \ln(\mathcal{Z}_{\Lambda\mathrm{CDM}}/\mathcal{Z}_{\omega_0\omega_a\mathrm{CDM}})$, computed with the *same* likelihood and nuisance parameter priors for both models (the only extension being ω_a). Following the Jeffreys scale (H. Jeffreys 1998), we interpret $|\ln \mathrm{BF}| < 1$ as inconclusive, $1 \leqslant |\ln \mathrm{BF}| < 2.5$ as weak evidence, $2.5 \leqslant |\ln \mathrm{BF}| < 5$ as moderate evidence, and $|\ln \mathrm{BF}| \geqslant 5$ as strong evidence. For our DESI DR2 splits, we find $\ln \mathrm{BF} = 2.41$, 2.06, 1.89, 0.10 for no LRG1, no LRG2, no LRG1 and LRG2, and full DR2, indicating weak evidence for ΛCDM in the first three cases and inconclusive support for the full sample. Hence, the data do not require the additional ω_a degree of freedom; the apparent trend toward $\omega_0 > -1$ with LRG1 included is best understood as prior volume sensitivity along the ω_0–ω_a ridge rather than a data-driven detection.

Our analysis uses the DESI BAO data only, so we can clearly see how each tracer affects the parameters. With DESI DR2 BAO alone, the $\omega_0\omega_a$CDM model is not well constrained. Stronger constraints require adding complementary data, for example, combining DESI DR2 with SNe Ia and the cosmic microwave background (CMB) (DESI DR2 + SNe Ia + CMB). Nevertheless, the predicted values of Ω_m in the LRG1 and LRG3+ELG1 tracers show strong disagreement with the Planck predictions, and when the LRG1 data point is included, DESI DR2 shows close agreement with the Planck-ΛCDM Ω_m predictions. One can conclude that the dynamic DE observed in the DESI DR2 data set is primarily influenced by the LRG1 and LRG2 data sets. Furthermore, the DESI DR2 paper provides strong evidence for dynamic DE. When the DESI DR2 data set is combined with other data sets, such as CMB, Pantheon$^+$, DESY5, and Union3 data sets, it seems to be partly due to a mismatch between BAO and SNe Ia measurements at lower redshifts ($z_{\mathrm{eff}} \sim 0.3$). Until the source of this discrepancy is better understood, claims of dynamic DE should be considered premature.

5 Discussion and Conclusions

The recent findings from the DESI DR2 data release suggest that the ΛCDM model is challenged by the combination of DESI DR2 BAO measurements and other observational data, motivating dynamical DE as a potential solution. Specifically, Figure 11 of M. A. Karim et al. (2025) shows that combining DESI DR2 with CMB data alone excludes ΛCDM at a significance of 3.1σ. When additional supernova data sets are included, the exclusion significances become 2.8σ with Pantheon$^+$, 3.8σ with Union3, and 4.2σ with DES-SN5YR. Similarly, Figure 5 highlights a preference for $\omega_0 > -1$ within the $\omega_0\omega_a$CDM model when the LRG1 and LRG2 data sets are included, showing that these two tracers in DESI DR2 preference $\omega_0 > -1$. Moreover, the dynamical DE signal in DR2 is actually the combination of a high Ω_m (LRG1), a lower Ω_m (LRG2), and a higher Ω_m at higher redshift.

The predicted value of Ω_m from DESI DR2 at $z_{\mathrm{eff}} = 0.510$ (LRG1) shows a tension of about 2.42σ with the ΛCDM Planck prediction (N. Aghanim et al. 2020). Similarly, the LRG3+ELG1 sample exhibits a 2.60σ tension relative to the Planck Ω_m value. These discrepancies place the DESI LRG1 and LRG3+ELG1 constraints in conflict not only with Planck but also with several SNe Ia samples (D. Brout et al. 2022; T. Abbott et al. 2024; D. Rubin et al. 2025). Moreover, all tracers except Lyα exhibit some level of tension. It is important to note that the effective redshift is quite similar across these data sets, although SNe Ia samples tend to be biased toward lower redshifts.

Furthermore, M. A. Karim et al. (2025) show that SDSS and DESI constraints are consistent with each other. Consequently, SDSS-IV also exhibits a similar trend, predicting a larger Ω_m within the same range (E. Ó Colgáin et al. 2022) (see Figure 5). Although the predicted value of Ω_m at $z_{\mathrm{eff}} = 0.51$ in the case of SDSS and DESI DR2 is very close, differences in Ω_m values between SDSS and DESI are noticeable at lower redshifts. While these differences may be attributed to systematics, they also suggest the possibility of statistical fluctuations in the data.

The success of the ΛCDM model is often highlighted by the consistent agreement across multiple observables, CMB, BAO, and SNe Ia, indicating that the Universe is composed of approximately 70% DE and 30% matter. In cosmology, it is essential that physical models are supported by a variety of independent observations; otherwise, the results may simply reflect statistical fluctuations or observational systematics. This concern is particularly relevant in the case of the LRG1 and LRG3+ELG1 constraints at $z_{\mathrm{eff}} = 0.510$ and $z_{\mathrm{eff}} = 0.934$, as well as the three SNe Ia samples. It should be noted that these SNe Ia samples are not fully independent from each other, raising the possibility that systematic effects persist across the samples. For instance, Pantheon$^+$ and Union3 share approximately 1360 SNe Ia, and Pantheon$^+$ and DES-SN5YR share 196 SNe Ia.

The key takeaway from this paper is that while it is possible to compare the behavior of different models, such as the $\omega_0\omega_a$CDM and ΛCDM models, we must ensure that the differences between these models are consistent across different types of measurements within the same redshift ranges. Without this consistency, claims of new physics remain unconvincing, regardless of the attention they may attract (G. Gu et al. 2024; O. Luongo & M. Muccino 2024; Y. Tada & T. Terada 2024; D. Wang 2024a; X. Wang et al. 2024; W. Yin 2024).

As shown in Table 2, the DESI DR2 data set exhibits a shift in the value of Ω_m of approximately 1.84σ as we move from lower to higher redshift bins. Specifically, Ω_m decreases with increasing effective redshift bin before rising again. Consequently, the parameter hr_d shows a negative correlation with Ω_m, leading to similar behavior of increasing and then decreasing values. SNe Ia measurements also exhibit similar trends (E. Ó Colgáin 2019; L. Kazantzidis et al. 2021). Indeed, this is not surprising, as large SNe Ia samples are typically compiled from several different surveys. As the number of surveys increases, observational systematics increase. However, recent studies have shown that the Pantheon$^+$ sample generally provides consistent Ω_m values (D. Brout et al. 2022), provided that high redshift SNe Ia are excluded (M. Malekjani et al. 2024). In contrast, DESI is based on a single survey, though it incorporates multiple tracers.

The main idea here is that ongoing tensions with the ΛCDM model, particularly the discrepancies in H_0 and $S_8 = \sigma_8\sqrt{\Omega_m/0.3}$ (E. Di Valentino et al. 2021b; E. Abdalla et al. 2022; L. Perivolaropoulos & F. Skara 2022), suggest that the model

may need to be revised if these tensions are found to be real. Such a revision could involve allowing cosmological parameters to evolve with effective redshift (C. Krishnan et al. 2021; C. Krishnan & R. Mondol 2023). While some may argue that the S_8 tension is merely a scale issue, as discussed in A. Amon & G. Efstathiou (2022) and C. Preston et al. (2023), this approach does not address the more statistically significant H_0 tension. Moreover, shifts in S_8 caused by changes in scale appear too small to fully resolve the S_8 tension (E. Di Valentino et al. 2021a; R. Terasawa et al. 2025). This reinforces the idea that the discrepancies in both H_0 and S_8 are not just scale effects, but may point to deeper issues within the ΛCDM model. Supporting evidence for this notion comes from various observations showing that H_0 decreases and Ω_m increases with increasing effective redshift, a trend reported in multiple studies (G. Risaliti & E. Lusso 2019; C. Krishnan et al. 2020; E. Lusso et al. 2020; M. Millon et al. 2020; A. J. Shajib et al. 2020; K. C. Wong et al. 2020; M. G. Dainotti et al. 2021; E. Ó Colgáin et al. 2022, 2024; J.-P. Hu & F.-Y. Wang 2022; J. Wagner 2022; M. G. Dainotti et al. 2022b, 2022c; X. Jia et al. 2023; P. L. Kelly et al. 2023; E. Pastén & V. H. Cárdenas 2023; M. Dainotti et al. 2023a; M. Malekjani et al. 2024; M. Pascale et al. 2025). If these findings hold, they could indicate that the ΛCDM model breaks down at the background level in the late Universe. Additionally, observations suggest that the S_8 tension, which seems to be a perturbative issue, is primarily located in the late Universe, especially at $z \lesssim 2$ (E. Abdalla et al. 2022; M. Esposito et al. 2022; S. A. Adil et al. 2024; M. S. Madhavacheril et al. 2024; I. Tutusaus et al. 2024; E. Di Valentino et al. 2025). For more details on the evidence supporting the evolution of ΛCDM parameters with redshift, refer to Ö. Akarsu et al. (2024).

DESI DR2 shows some improvement when compared to previous data, but the situation remains uncertain due to the persistence of the anomaly in the LRG1 ($z_{\rm eff} = 0.51$) and LRG3+ELG1 ($z_{\rm eff} = 0.943$) data sets. This anomaly could lead to discrepancies between BAO, CMB + SNe Ia measurements, and possibly even between CMB and SNe Ia data (T. Abbott et al. 2024), particularly regarding Ω_m. On the other hand, if the data quality improves and the tension with Planck, Pantheon$^+$, and other measurements is reduced, it is possible that the negative correlation between Ω_m and hr_d at lower redshifts could disappear. Instead, we may observe the more typical trend of increasing Ω_m and decreasing H_0, which reflects a negative correlation between Ω_m and H_0. In a follow-up paper, we aim to explore various DE models and check whether the DESI LRG1 analogy holds and can be improved in all these models.

In our next paper, we intend to extend the above analysis and investigate these effects in greater depth, as it is important to recognize the statistical limitations of tracer-wise inference. Each DESI tracer provides only a small number of BAO observables (e.g., D_H/r_d, D_M/r_d, D_V/r_d, D_M/D_H), while models such as ΛCDM and $\omega_0\omega_a$CDM involve several free parameters. This imbalance makes individual tracer fits inherently underconstrained and prone to amplifying parameter degeneracies, particularly among Ω_m, H_0, and r_d. Apparent redshift-dependent trends or tensions may therefore arise from statistical fluctuations or prior volume effects rather than genuine signs of new physics. A more robust picture emerges only when combining tracers and cross-checking with complementary probes such as the CMB or SNe Ia, which we plan to pursue in our upcoming work.

Acknowledgments

S.C. acknowledges the Istituto Nazionale di Fisica Nucleare (INFN) Sez. di Napoli, Iniziative Specifiche QGSKY and MoonLight-2 and the Istituto Nazionale di Alta Matematica (INdAM), gruppo GNFM, for the support. This paper is based on work from COST Action CA21136–Addressing observational tensions in cosmology with systematics and fundamental physics (CosmoVerse), supported by COST (European Cooperation in Science and Technology). V.K.S. gratefully acknowledges the facilities and institutional support provided by the Indian Institute of Astrophysics (IIA), India, during his tenure as a postdoctoral fellow. G. Mustafa is very thankful to Prof. Gao Xianlong from the Department of Physics, Zhejiang Normal University, for his kind support and help during this research.

ORCID iDs

Himanshu Chaudhary https://orcid.org/0000-0002-6376-0707
Salvatore Capozziello https://orcid.org/0000-0003-4886-2024
Vipin Kumar Sharma https://orcid.org/0000-0001-7640-5504
Ghulam Mustafa https://orcid.org/0000-0003-1409-2009

References

Abbott, T., Acevedo, M., Aguena, M., et al. 2024, ApJL, 973, L14
Abdalla, E., Abellán, G. F., Aboubrahim, A., et al. 2022, JHEAp, 34, 49
Adame, A. G., et al. 2025, JCAP, 02, 021
Adil, S. A., Akarsu, Ö., Malekjani, M., et al. 2024, MNRAS: Letters, 528, L20
Aghanim, N., Akrami, Y., Ashdown, M., et al. 2020, A&A, 641, A6
Akarsu, Ö., Ó Colgáin, E., Sen, A. A., Sheikh-Jabbari, M., et al. 2024, Univ, 10, 305
Alam, S., Ata, M., Bailey, S., et al. 2017, MNRAS, 470, 2617
Alam, S., Aubert, M., Avila, S., et al. 2021, PhRvD, 103, 083533
Alfano, A. C., Capozziello, S., Luongo, O., & Muccino, M. 2024, JHEAp, 42, 178
Amon, A., & Efstathiou, G. 2022, MNRAS, 516, 5355
Aubourg, É., et al. 2015, PhRvD, 92, 123516
Bamba, K., Capozziello, S., Nojiri, S., & Odintsov, S. D. 2012, Ap&SS, 342, 155
Bargiacchi, G., Benetti, M., Capozziello, S., et al. 2022, MNRAS, 515, 1795
Bargiacchi, G., Dainotti, M., Nagataki, S., & Capozziello, S. 2023, MNRAS, 521, 3909
Bargiacchi, G., Dainotti, M. G., & Capozziello, S. 2025, NewAR, 100, 101712
Benetti, M., Bargiacchi, G., Risaliti, G., et al. 2025, PDU, 49, 101983
Brout, D., Scolnic, D., Popovic, B., et al. 2022, ApJ, 938, 110
Calderon, R., et al. 2024, JCAP, 10, 048
Camarena, D., Greene, K., Houghteling, J., & Cyr-Racine, F.-Y. 2025, arXiv:2507.17969
Chevallier, M., & Polarski, D. 2001, IJMPD, 10, 213
Chudaykin, A., Dolgikh, K., & Ivanov, M. M. 2021, PhRvD, 103, 023507
Cortês, M., & Liddle, A. R. 2024, JCAP, 2024, 007
Dainotti, M., De Simone, B., Montani, G., Schiavone, T., & Lambiase, G. 2023a, arXiv:2301.10572
Dainotti, M., Lenart, A. Ł., Chraya, A., et al. 2023b, MNRAS, 518, 2201
Dainotti, M. G., Bargiacchi, G., Lenart, A. Ł., & Capozziello, S. 2024a, Galax, 12, 4
Dainotti, M. G., Bargiacchi, G., Lenart, A. Ł., Nagataki, S., & Capozziello, S. 2023c, ApJ, 950, 45
Dainotti, M. G., Bargiacchi, G., Lenart, A. Ł., et al. 2022a, ApJ, 931, 106
Dainotti, M. G., Cardone, V. F., & Capozziello, S. 2008, MNRAS: Letters, 391, L79
Dainotti, M. G., De Simone, B., Schiavone, T., et al. 2021, ApJ, 912, 150
Dainotti, M. G., De Simone, B., Schiavone, T., et al. 2022b, Galax, 10, 24
Dainotti, M. G., Lenart, A., Yengejeh, M. G., et al. 2024b, PDU, 44, 101428
Dainotti, M. G., Sarracino, G., & Capozziello, S. 2022c, PASJ, 74, 1095
Demianski, M., Piedipalumbo, E., Sawant, D., & Amati, L. 2017, A&A, 598, A112
Di Valentino, E., et al. 2021a, APh, 131, 102604
Di Valentino, E., et al. 2025, Phys. Dark Univ, 49, 101965
Di Valentino, E., Mena, O., Pan, S., et al. 2021b, CQGra, 38, 153001

Eisenstein, D. J., et al. 2005, ApJ, 633, 560
Escamilla-Rivera, C., & Capozziello, S. 2019, IJMPD, 28, 1950154
Esposito, M., Iršič, V., Costanzi, M., et al. 2022, MNRAS, 515, 857
Goldstein, S., Celoria, M., & Schmidt, F. 2025, arXiv:2507.16970
Gu, G., Wang, X., Mu, X., Yuan, S., & Zhao, G.-B. 2024, RAA, 24, 065001
Handley, W., Hobson, M., & Lasenby, A. 2015a, MNRAS: Letters, 450, L61
Handley, W., Hobson, M., & Lasenby, A. 2015b, MNRAS, 453, 4384
Hu, J.-P., & Wang, F.-Y. 2022, MNRAS, 517, 576
Jedamzik, K., Pogosian, L., & Zhao, G.-B. 2021, CmPhy, 4, 123
Jeffreys, H. 1998, The Theory of Probability (Oxford: Oxford Univ. Press)
Jia, X., Hu, J., & Wang, F. 2023, A&A, 674, A45
Karim, M. A., Aguilar, J., Ahlen, S., et al. 2025, arXiv:2503.14738,
Kazantzidis, L., Koo, H., Nesseris, S., Perivolaropoulos, L., & Shafieloo, A. 2021, MNRAS, 501, 3421
Kelly, P. L., Rodney, S., Treu, T., et al. 2023, Sci, 380, eabh1322
Khadka, N., Luongo, O., Muccino, M., & Ratra, B. 2021, JCAP, 2021, 042
Khadka, N., & Ratra, B. 2020, MNRAS, 497, 263
Khadka, N., & Ratra, B. 2021, MNRAS, 502, 6140
Krishnan, C., Ó Colgáin, E., Ruchika, S. A. A., Sheikh-Jabbari, M., & Yang, T. 2020, PhRvD, 102, 103525
Krishnan, C., & Mondol, R. 2023, Cosmology Workshop on A Multipolar Universe (Berlin: Springer)
Krishnan, C., Ó Colgáin, E., Sheikh-Jabbari, M., & Yang, T. 2021, PhRvD, 103, 103509
Lenart, A. Ł., Bargiacchi, G., Dainotti, M. G., Nagataki, S., & Capozziello, S. 2023, ApJS, 264, 46
Lewis, A. 2025, JCAP, 2025, 025
Li, X., & Liao, K. 2024, ApJ, 966, 121
Lin, W., Chen, X., & Mack, K. J. 2021, ApJ, 920, 159
Linder, E. V. 2003, PhRvL, 90, 091301
Lodha, K., et al. 2025, PhRvD, 111, 023532
Luongo, O., & Muccino, M. 2024, A&A, 690, A40
Lusso, E., Risaliti, G., Nardini, E., et al. 2020, A&A, 642, A150
Madhavacheril, M. S., Qu, F. J., Sherwin, B. D., et al. 2024, ApJ, 962, 113
Malekjani, M., Mc Conville, R., Ó Colgáin, E., Pourojaghi, S., & Sheikh-Jabbari, M. 2024, EPJC, 84, 317
Millon, M., Galan, A., Courbin, F., et al. 2020, A&A, 639, A101
Notari, A., Redi, M., & Tesi, A. 2025, JCAP, 04, 048
Ó Colgáin, E. 2019, JCAP, 2019, 006
Ó Colgáin, E., Dainotti, M. G., Capozziello, S., et al. 2026, JHEAp, 49, 100428
Ó Colgáin, E., Pourojaghi, S., Sheikh-Jabbari, M., & Yin, L. 2025, arXiv:2504.04417
Ó Colgáin, E., Sheikh-Jabbari, M., Solomon, R., et al. 2022, PhRvD, 106, L041301
Ó Colgáin, E., Sheikh-Jabbari, M., Solomon, R., Dainotti, M. G., & Stojkovic, D. 2024, PDU, 44, 101464
Park, C.-G., de Cruz Pérez, J., & Ratra, B. 2025, Int. J. Mod. Phys. D, 34, 2550058
Pascale, M., Frye, B. L., Pierel, J. D., et al. 2025, ApJ, 979, 13
Pastén, E., & Cárdenas, V. H. 2023, PDU, 40, 101224
Percival, W. J., et al. 2010, MNRAS, 401, 2148
Perivolaropoulos, L., & Skara, F. 2022, NewAR, 95, 101659
Perlmutter, S., et al. 1999, ApJ, 517, 565
Petrosian, V., Singal, J., & Mutchnick, S. 2022, ApJL, 935, L19
Pogosian, L., Zhao, G.-B., & Jedamzik, K. 2020, ApJL, 904, L17
Pogosian, L., Zhao, G.-B., & Jedamzik, K. 2024, ApJL, 973, L13
Pourojaghi, S., Zabihi, N., & Malekjani, M. 2022, PhRvD, 106, 123523
Preston, C., Amon, A., & Efstathiou, G. 2023, MNRAS, 525, 5554
Riess, A. G., et al. 1998, AJ, 116, 1009
Risaliti, G., & Lusso, E. 2019, NatAs, 3, 272
Rubin, D., Aldering, G., Betoule, M., et al. 2025, ApJ, 986, 231
Sahni, V., & Starobinsky, A. 2006, IJMPD, 15, 2105
Shajib, A. J., Birrer, S., Treu, T., et al. 2020, MNRAS, 494, 6072
Sharma, V. K., Chaudhary, H., & Kolekar, S. 2025, arXiv:2507.00835
Singal, J., Mutchnick, S., & Petrosian, V. 2022, ApJ, 932, 111
Sousa-Neto, A., Bengaly, C., Gonzalez, J. E., & Alcaniz, J. 2025, arXiv:2502.10506
Srinivasaragavan, G. P., Dainotti, M. G., Fraija, N., et al. 2020, ApJ, 903, 18
Tada, Y., & Terada, T. 2024, PhRvD, 109, L121305
Terasawa, R., Li, X., Takada, M., et al. 2025, PhRvD, 111, 063509
Tutusaus, I., Bonvin, C., & Grimm, N. 2024, NatCo, 15, 9295
Vagnozzi, S. 2023, Univ, 9, 393
Vilardi, S., Capozziello, S., & Brescia, M. 2025, A&A, 695, A166
Wagner, J. 2022, arXiv:2203.11219
Wang, D. 2024a, arXiv:2404.06796
Wang, D. 2024b, arXiv:2404.13833
Wang, X., Gu, G., Mu, X., Yuan, S., & Zhao, G.-B. 2024, RAA, 24, 065002
Weinberg, S. 1989, RvMP, 61, 1
Wolf, W. J., Ferreira, P. G., & García-García, C. 2025a, PhRvD, 111, L041303
Wolf, W. J., García-García, C., & Ferreira, P. G. 2025b, JCAP, 2025, 034
Wong, K. C., Suyu, S. H., Chen, G. C., et al. 2020, MNRAS, 498, 1420
Yin, W. 2024, JHEP, 2024, 1
Zajaček, M., Czerny, B., Khadka, N., et al. 2024, ApJ, 961, 229
Zel'dovich, Y. B. 1968, SvPhU, 11, 381